A microglial cell model for acyl-CoA oxidase 1 deficiency

Q. Raas[1], F-E. Saih[1,2], C. Gondcaille[1], D. Trompier[1], Y. Hamon[3], V. Leoni[4], C. Caccia[5], B. Nasser[2], M. Jadot[6], F. Ménétrier[7], G. Lizard[1,8], M. Cherkaoui-Malki[1], P. Andreoletti[1], S. Savary[1]*

[1]Laboratoire Bio-PeroxIL EA7270, University of Bourgogne Franche-Comté, Dijon, France,
[2]Laboratoire de Biochimie et Neurosciences, Faculté des Sciences et Techniques, University Hassan I, Settat, Morocco,
[3]Aix Marseille Univ, CNRS, INSERM, CIML, Centre d'Immunologie de Marseille-Luminy, Marseille, France,
[4]Laboratory of Clinical Chemistry, Hospital of Varese, ASST-Settelaghi, Milan, Italy,
[5]Laboratory of Medical Genetics and Neurogenetics, Foundation IRCCS Istituto Neurologico Carlo Besta, Milan, Italy,
[6]Unité de Recherche en Physiologie Moléculaire (URPhyM), laboratoire de Chimie Physiologique, NARILIS (Namur Research Institute for Life Sciences), University of Namur (UNamur), Namur, Belgium,
[7]Centre des Sciences du Goût et de l'Alimentation, AgroSup Dijon, UMR6265/UMRA1324, CNRS, INRA, University of Bourgogne Franche-Comté, Dijon, France,
[8]INSERM, Dijon, France.

Footnotes
* Corresponding author: Tel.: +33 (0)380396273. Fax: +33 (0)380396250. E-mail address: stsavary@u-bourgogne.fr

Abbreviations: ACOX1, acyl-CoA oxidase 1; copGFP, copepod green fluorescent protein; CRISPR, clustered regularly interspaced short palindromic repeat; DAB, diaminobenzidine; FBS, fetal bovine serum; GC-MS, gas chromatography mass spectrometry; GFP, green fluorescent protein; HDR, homologous directed repair; NAD, nicotinamide adenine dinucleotide; L/VLCFA, long/very long-chain fatty acids; MUFA, monounsaturated fatty acids; NHEJ, non-homologous end-joining; PUFA, polyunsaturated fatty acids; SFA, saturated fatty acids; TEM, transmission electron microscopy; TK, thymidine kinase.

Keywords: peroxisome, microglia, acyl-CoA oxidase, VLCFA

Abstract
Acyl-CoA oxidase (ACOX1) deficiency is a rare and severe peroxisomal leukodystrophy associated with a very long-chain fatty acid (VLCFA) β–oxidation defect. This neurodegenerative disease lacks relevant cell models to further decipher the pathomechanisms in order to identify novel therapeutic targets. Since peroxisomal defects in microglia appear to be a key component of peroxisomal leukodystrophies, we targeted the *Acox1* gene in the murine microglial BV-2 cell line. Using CRISPR/Cas9 gene editing, we generated an *Acox1*-deficient cell line and validated the allelic mutations, which lead to the absence of ACOX1 protein and enzymatic activity. The activity of catalase, the enzyme degrading H_2O_2, was increased, likely in response to the alteration of redox homeostasis. The mutant cell line grew more slowly than control cells without obvious morphological changes. However, ultrastructural analysis revealed an increased number of peroxisomes and mitochondria associated with size reduction of mitochondria. Changes in the distribution of lipid droplets containing neutral lipids have been observed in mutant cells; lipid analysis revealed the accumulation of saturated and

monounsaturated VLCFA. Besides, expression levels of genes encoding interleukin-1 beta and 6 (*IL-1β* and *IL-6*), as well as triggering receptor expressed on myeloid cells 2 (*Trem2*) were found modified in the mutant cells suggesting modification of microglial polarization and phagocytosis ability. In summary, this *Acox1*-deficient cell line presents the main biochemical characteristics of the human disease and will serve as a promising model to further investigate the consequences of a specific microglial peroxisomal β–oxidation defect on oxidative stress, inflammation and cellular functions.

1. Introduction

Peroxisomes are small organelles (0.1-1 µm), found in almost all cell types, that take their name from their capacity to produce and convert hydrogen peroxide into water. Many severe genetic disorders have been associated to a peroxisomal biogenesis defect or a single peroxisomal deficiency illustrating their vital function in cells and tissues [1]. One of their main roles concerns lipid metabolism, especially oxidation of fatty acids. Peroxisomal β–oxidation, which consists of a 4-step enzymatic loop, permit to shorten fatty acids by 2 carbon atoms at each cycle along with the release of one acetyl-CoA molecule [2]. Peroxisomal acyl-coenzyme A oxidase 1 (ACOX1, E.C. 1.3.3.6) catalyzes the first and rate-limiting step of this β–oxidation pathway dedicated to straight-chain fatty acids, which includes long- and very long-chain fatty acids (LCFA, VLCFA), polyunsaturated fatty acids, and dicarboxylic acids. Peroxisomal oxidation of bile acid intermediates depends on ACOX2 [3] while oxidation of branched-chain fatty acids depends on both ACOX2 and ACOX3 enzymes [4, 5]. The reaction catalyzed by ACOX1 consists of dehydrogenation of acyl-CoA to 2-trans-enoyl-CoA and produces hydrogen peroxide which is subsequently transformed into water and oxygen by catalase. In human and mice, the ACOX1 enzyme is encoded by a single gene localized on chromosome 17 and 11 respectively [6-9]. Alternative splicing leads to the synthesis of two protein isoforms ACOX1a or ACOX1b with different substrate specificity [10].

Growth retardation, sterility, and hepatomegaly with steatosis, were described in *Acox1*-deficient mice [11]. Although ACOX1 is widely expressed in the brain [12, 13], its absence in null mice did not lead to apparent neurological manifestations. In human, however, ACOX1 deficiency (OMIM #264470) is associated with very severe and generalized neurological alterations (average age of death: 5 years). This rare autosomal disorder (about 30 patients have been reported worldwide) also known as pseudo-neonatal adrenoleukodystrophy, is characterized by infantile-onset hypotonia, seizures, visual impairment, loss of motor achievements and progressive white and gray matter degeneration resembling neonatal adrenoleukodystrophy [7, 14-17]. Similar demyelination observations were obtained after experimental inhibition of peroxisomal β–oxidation in rat brain [18]. Hepatomegaly, adrenal insufficiency and craniofacial dysmorphia are less frequently reported. Biochemically, the disease is characterized by the accumulation of both saturated and monounsaturated VLCFA while plasma levels of branched-chain fatty acids and bile acid intermediates as well as erythrocytes plasmalogens remain unchanged. The monitoring of VLCFA levels and their ratios (C26:0/C22:0 or C24:0/C22:0) is indeed used for diagnosis in complement of magnetic resonance imaging and genetic analysis [16, 19, 20].

The in-depth characterization of fibroblasts of patients with ACOX1 deficiency has established a link between peroxisomal defect and inflammation [21]. Although the inflammatory component represents a major feature of the disease, increased oxidative stress, endoplasmic reticulum stress as well as altered brain cellular crosstalk are strongly suspected to contribute to the development of neuroinflammation and neurodegenerative processes. Selective ablation of functional peroxisomes in brain cell lineages using specific *Pex5* knockout mice has underlined the importance of the cellular context [22, 23]. This is especially true in

oligodendrocytes, the myelin producing cells [24]. In other peroxisomal leukodystrophies such as X-linked adrenoleukodystrophy, peroxisomal alterations and VLCFA accumulation in microglial cells have been proposed to trigger inflammatory processes and increased oxidative stress that contribute to amplifying the primary peroxisomal defect [25, 26]. Microglia was indeed identified as a main actor in the phagocytosis of myelin debris along with secretion of neuroprotective molecules [27]. It can therefore be assumed that a peroxisomal defect in the microglia would trigger a gradual loss of its ability to eliminate damaged myelin and, consequently, to scavenge the lipotoxic effects of VLCFA in other brain cell types.

The study of the physiopathogenesis of ACOX1 deficiency and the identification of underlying neurodegenerative and inflammatory processes require the development of relevant study models. Skin fibroblasts are usually the only *in vitro* model for peroxisomal diseases. The recent emergence of clustered regularly interspaced short palindromic repeat (CRISPR)/CRISPR-associated protein 9 (Cas9) gene editing methodologies now offers the opportunity to target any gene in almost any cell types [28]. Specific CRISPR/Cas9-mediated double strand DNA break can be obtained in a specific gene using a single guide RNA (sgRNA). The selection of homologous directed repair (HDR), if a donor sequence is present in the cells, or non-homologous end-joining (NHEJ) repair events allows targeted mutations to be obtained. Microglia being considered as a key cell type in brain pathology, we decided to generate a murine microglial cell line bearing *Acox1* mutation using CRISPR/Cas9 gene editing strategy. The BV-2 immortalized cell line, established in 1990 [29], benefits from a huge scientific background and is extensively used as a good alternative to primary microglial cells in the context of neurodegenerative researches. Indeed, this cell line retains most of the morphological, phenotypical and functional properties described for freshly isolated microglial cells [30]. Moreover, BV-2 cells share properties with macrophages with respect to the antigen profile, phagocytic capacity and antimicrobial activity and retain the potential for inflammatory cytokine secretion [31]. Here, we describe the establishment of an *Acox1*-deficient BV-2 cell clone, its validation and its characterization focusing on cell growth, cell morphology and ultrastructure, and fatty acid content.

2. Materials and methods

2.1. Plasmids

Custom synthesized plasmids used for genome editing were obtained from GeneCopoeia, Inc/tebu-bio (France). The all-in-one plasmid (Catalog No: MCP231241-CG01-2-B-b) enables the co-expression of a sgRNA targeting the first exon of the *Acox1* gene (target sequence: 5'- GGCCCGCTCCTTGCGCAGAT -3') under the regulation of a U6 promoter and a Cas9 nuclease driven by a CMV promoter. The specificity of CRISPR/Cas9 editing mainly depends on the sgRNA sequence and on the presence of protospacer adjacent motif located next to the target sequence. Potential off-target cleavage activity has already been described in sequences presenting three to five mismatches with the sequence of the sgRNA [32]. To avoid non-specific mutations, we paid attention to the design of the all-in-one CRISPR plasmid and relied on the expertise of our plasmid supplier (GeneCopoeia, Inc). The sgRNA sequence targeting the first exon of *Acox1* was chosen to exhibit the highest quality score by inverse likelihood of off-target binding based on the CRISPR design tool developed by Zhang Lab, MIT 2017 (http://crispr.mit.edu/). To test for potential off-target mutations on the selected knockout cell clone, we looked for NHEJ-mediated mutations on the two genomic sites of the 56 potential sites displaying the highest predicted likelihood of off-target binding (Table 1). Sanger sequencing confirmed the absence of CRISPR/Cas9-induced mutations in these putative targets located on chromosomes X and 12 respectively (data not shown), strongly suggesting the absence of off-target events.

The donor plasmid (DC-MTN231241-D07), contains two recombination arms flanking the genomic cutting site and selection cassettes (copGFP and puromycin resistance) flanked by two LoxP sites. The donor plasmid also contains a thymidine kinase (TK) cassette outside of the recombination arms conferring ganciclovir sensitivity in case of random integration.

The plasmid pOG231 (Addgene), a Cre-expressing plasmid for removal of floxed sequences, was kindly provided by M. Baes (Leuven, Belgium).

2.2. Cell culture, transfection, clonal selection, and proliferation assay

Murine microglial cells (BV-2) from Banca-Biologica e Cell Factory (catalog no. ATL03001) were cultured in DMEM supplemented with 10% heat-inactivated FBS and 1% penicillin/streptomycin (Dutscher). Cultures were maintained at 37°C in a humidified atmosphere containing 5% CO_2.

BV-2 cells ($2x10^6$, ~70% confluence) were transfected with 2 µg all-in-one plasmid and 2 µg donor plasmid using Amaxa Cell Line Nucleofector Kit T (Lonza) and program A-023, to allow CRISPR/Cas9-primed homologous directed repair (HDR). Recombinant cells were treated 48 h after transfection with puromycin 3 µg/ml for 19 days (positive selection). Negative selection of potential non-targeted integration started 11 days after transfection. Ganciclovir (2 µM) was added to the culture for 12 days. After antibiotic selection, cells were sorted by flow cytometry based on high expression of copGFP and then seeded as single cells in a 96-well plate. Cells were allowed to grow for 10-14 days before genotyping. In order to remove the selection cassettes, the validated clones were transfected with 2 µg Cre-expressing plasmid using Amaxa Cell Line Nucleofector Kit T (Lonza) and program A-023. 48 h after transfection, cells with no expression of copGFP were sorted by flow cytometry and then seeded as single cells in a 96-well plate.

For growth comparison, WT and mutant BV-2 cells were seeded in 24-well plates ($2x10^4$ cells/well) and cultivated for 24, 48, 72 or 96 h. The cells being semi-adherent, the medium was not replaced during growth to avoid cell loss. Viability was evaluated with trypan blue (0.025% final concentration). Living cells were counted using a hemocytometer. The average number of cells was obtained from 3 independent wells.

2.3. Molecular analysis (Genomic DNA purification, PCR)

Genomic DNA was extracted from selected clones with the Wizard Genomic DNA Purification Kit (Promega) and PCR amplified with the GoTaq Long PCR master mix (Promega) using the following primers *Acox1*F: 5'- CTCAAGGCCCTGGCCAATCG -3', *Acox1*R: 5'-ACGCCCATCGAAGTAGGGGT-3'. To control targeted recombination, PCR products were visualized on a 1% agarose electrophoresis gel using a Bio-Rad Gel Doc XR+ Imager System. NHEJ mediated mutations were confirmed after PCR amplification with the same primers and a GoTaq Flexi DNA polymerase (Promega) (unable to amplify fragments longer than 2 kb), and Sanger sequencing (Eurofins Genomics sanger sequencing platform, Germany).

2.4. Western blotting

Cell lysates were prepared in solubilization buffer containing 100 mM Tris-HCl, pH 8, 100 mM NaCl, 1% Triton X-100, 1% PMSF, and cOmplete protease inhibitor mixtures (Roche Applied Science). Proteins from total cell lysate (50 µg) were separated on 7.5% SDS-PAGE and transferred onto a PVDF membrane. First incubated in 5% skimmed milk in PBS, 0.1% Tween 20 (PBS/T) for 1 h at room temperature, the membrane was then probed with mouse anti-actin antibody (dilution 1:10,000; Sigma-Aldrich) or a home-made rabbit polyclonal antibody raised against the purified 72 kDa polypeptide of rat ACOX1 [33]. Following the incubation with the appropriate horseradish peroxidase (HRP)-conjugated secondary antibody

(1:5,000; Santa Cruz Biotechnology, Inc.), immunoreactivity was revealed by ECL (Santa Cruz Biotechnology). The membrane was first probed with the anti-ACOX1 antibody and then stripped by incubation for 30 min in stripping buffer (62.5 mM Tris-HCl, 2% SDS, 100 mM β-mercaptoethanol) before being probed with the anti-actin antibody. Image processing and analysis were obtained using a Bio-Rad-Chemidoc XRS system and the Image Lab version 4.0 software for quantitative analysis.

2.5. Enzymatic activities

To monitor peroxisomal β-oxidation, cyanide-insensitive palmitoyl-CoA oxidation enzyme activity was measured through its ability to elicit the reduction of NAD as previously described [34]. Briefly, 25 µl of BV-2 cell lysate was preincubated at 37°C with a 450 µl mixture containing 50 mM phosphate buffer (pH 7.4), 12 mM DL-dithiothreitol (DTT), 200 µg/ml bovine serum albumin (fatty acid free), 0.2 mM β-nicotinamide adenine dinucleotide hydrate (NAD), and 1 mM potassium cyanide freshly prepared. The reaction was initiated with the addition of 50 mM palmitoyl coenzyme A lithium salt (all reagents were from Sigma-Aldrich). The reduction of NAD^+ was monitored at 37°C by spectrophotometry at 340 nm during 20 min. The initial reaction rate was expressed in µmol/min of reduced NAD^+ and was reported to the mass of protein in mg.

Catalase enzyme assay was adapted from the method described by Ni et al. (2001) to be performed in 96-well plate [35]. Briefly, 10 µl of BV-2 cell lysate was added to 190 µl of 50 mM Tris HCl buffer (pH 7.4) containing 20 mM H_2O_2 (Sigma-Aldrich). The decrease of the absorbance was monitored at 240 nm for 2 min using Infinite M200 Pro spectrophotometer (TECAN Lyon, France). The linearity of absorbance as function of time was proportional to the breakdown of H_2O_2. The catalase activity was expressed as µmol/min/mg of protein.

2.6. Optic and electron microscopy

The content of cellular neutral lipids was evaluated by staining cells with Oil Red O (Sigma-Aldrich). A 0.5% Oil Red O solution was prepared in 100% propylene glycol by heating to 95°C, then filtered (Whatman filter paper), left over night at room temperature and filtered again (Whatman filter paper) just before use. BV-2 cells were seeded onto cover-slips in 24-well plate (10^5 cells/well) and grown for 24h. After 3 PBS rinses, cells were fixed in 4% paraformaldehyde for 10 min, washed with deionized water 3 times for 1 min per rinse, and stained with Oil Red O for 15 min. To remove Oil Red O excess, cells were washed with 60% propylene glycol 1 time for 1 min then with deionized water 4 times for 30 sec per rinse. The cover-slips were air dried and mounted in water-based preservative medium (Dako). Cells were observed using an Axioscope A1 light microscope (Zeiss).

Transmission electron microscopy was used to visualize WT and *Acox1*-deficient BV-2 cells cultured for 24 h. For the peroxisomal localization, cells were fixed for 1 h at 4°C in 2.5% (w/v) glutaraldehyde diluted in 0.1 M cacodylate buffer (pH 7.4), washed in 0.1 M cacodylate buffer (pH 7.4), incubated in the dark for 1 h at 21°C in 0.05 M Tris–HCl (pH 9.0) containing diaminobenzidine (2.5 mg/ml) and H_2O_2 (10 µl/ml of a 3% solution), washed in 0.1 M cacodylate buffer (pH 7.4) for 5 min at 21°C, post-fixed in 1% (w/v) osmium tetroxide diluted in 0.1 M cacodylate sodium buffer (pH 7.4) for 1 h at 21°C in the dark, and rinsed in 0.1 M cacodylate buffer (pH 7.4). The preparations were then dehydrated in graded ethanol solutions and embedded in Epon resin. Ultra-thin sections were cut with an ultramicrotome, contrasted with uranyl acetate and lead citrate, and examined under an H7500 electron microscope (Hitachi, Tokyo, Japan).

Micrographs corresponding to 12 cells for each genotype, randomly taken from the grid, were analyzed by 6 different investigators in blind with a particular focus on the number of peroxisomes, mitochondria, and lipid vesicles to give a score for each feature. Statistical

analysis was performed from the analytical scores. Morphometry was performed from micrographs form 12 cells using ImageJ calculation of areas after manual delineation of organelles. The mean area (+/- SD) was expressed in μm^2 and the maximum and minimum sizes were noted.

2.7. Fatty acid analysis

Cellular homogenates, prepared from pellets of 10^7 cells suspended in water (100 µl) and sonicated for 10 minutes, were added to a screw-capped vial sealed with a Teflon septum together with structural homologous internal standards (pentadecanoic and heptadecanoic acid), butylated hydroxytoluene and EDTA and flushed with argon for 10 min to remove air. Alkaline hydrolysis was allowed to proceed at room temperature (22°C) with magnetic stirring for 60 minutes in the presence of ethanolic 0.5 M potassium hydroxide solution. Fatty acids were collected by liquid to liquid extraction after correction of pH (<3) with HCl. All metabolites were extracted in sequential liquid to liquid extraction with hexane and ethylacetate. The organic solvents were evaporated under a gentle stream of argon and converted into trimethylsilyl ethers with bis(trimethylsilyl)trifluoroacetamide with 1% trimethylchlorosilane (Pierce).

Gas chromatography mass spectrometry (GC-MS) analysis was performed on a Clarus 600D (Perkin Elmer, USA). The GC was equipped with an Elite column (30m x 0.32mm id x 0.25 mm film; Perkin Elmer, USA) and injection was performed in splitless mode using helium (1 ml/min) as carrier gas. The temperature program was as follows: initial temperature of 80°C was held for 1 min, followed by a linear ramp of 10°C/min to 240°C, 20°C/min to 280°C and 5°C/min up to 290°C, which was held for 8 min.

The mass spectrometer operates in full mass scan mode. Peak integration was performed manually, and metabolites were recognized by retention time and fragmentation patterns and quantified from total-ion count against internal standards using standard curves for the measured fatty acids.

2.8. RTqPCR analysis

Total RNA were isolated from cells and treated with DNase using the "RNeasy Mini kit" (Qiagen). After quality and quantity control by spectrophotometry, RNA (1 µg) were reverse transcribed using the "iScript cDNA synthesis kit" (Bio-Rad). The synthesized cDNA were used as a template for Real-time PCR analysis using the SYBR Green real-time PCR technology and a StepOne Plus system (Applied Biosystems) as previously described [36]. *IL-1β*, *IL-6* and *Trem2* expression was quantified relatively to the expression of the house-keeping gene *36B4* using the following primers: *IL-1β*: F, 5'-AAGGAGAACCAAGCAACGAC-3', R, 5'-GAGATTGAGCTGTCTGCTCA-3', *IL-6*: F, 5'-GTTCTCTGGGAAATCGTGGA-3', R, 5'-TGTACTCCAGGTAGCTATGG-3', *Trem2*: F, 5'-GACCTCTCCACCAGTTTCTCC-3', R, 5'-TACATGACACCCTCAAGGACTG-3', *36B4*: F, 5'-ATGGGTACAAGCGCGTCCTG-3', R, 5'-GCCTTGACCTTTTCAGTAAG-3'.

2.9. Statistical analysis

Statistical analysis was performed using GraphPad Prism 5 software. Two-way repeated measure ANOVA followed by a Bonferronni post hoc test was used for growth curve comparison while t-tests were used when comparing only two groups. In all statistical tests, values of $p<0.05$ were considered significant.

3. Results

3.1. Isolation and validation of a novel Acox1-deficient BV-2 cell line

BV-2 cells were co-transfected with 2 plasmids designed to target the first exon of the *Acox1* gene. The first plasmid was designed to produce an *Acox1*-specific sgRNA and to express the nuclease Cas9. The second plasmid was a donor plasmid containing *Acox1* homologous arms for homologous directed recombination repair (HDR) after double-strand break (Fig. 1A). The plasmid also contains floxed selection cassettes for puromycin resistance and copGFP expression as well as an external TK cassette for negative selection. Transfected cells were first submitted to puromycin selection for 19 days. At day 11, negative selection with gancyclovir was started to remove random integration events. At the end of selection, cells were clonally sorted by flow cytometry.

The genotype of the 52 obtained cell clones was first checked by PCR and revealed a successful HDR for a dozen clones (Fig. 1B). The recombination event introduces a substantial mutation in the first exon of the *Acox1* gene, sufficient to inactivate the gene. However, the presence of a second shorter band on the gel corresponding to a non-recombinant locus indicated that the HDR was only monoallelic. Sanger sequencing of the second allele in the 12 cell clones demonstrated the presence of the same single insertion at the targeted site (T insertion into the fifth codon of the coding sequence) resulting in a frame shift a few nucleotides after the initiation codon (Fig. 1C). One of the cell clones containing these two mutations, respectively due to HDR and NHEJ, was transfected with a Cre recombinase expression vector to remove the selection cassettes. The further clonal selection of the transfected cells led to isolate an *Acox1* knock out subclone whose removal of selection cassettes was confirmed by PCR (Fig. 1B, lane 4) and sequencing (Fig. 1C). At the end of each step, mutant cell clones were amplified to generate a stock of cryogenic vials at the lowest passage.

Two mutated alleles resulting from HDR and Cre recombination and from the single insertion in the beginning of the coding sequence being present, a full inactivation of the *Acox1* gene without interference with transcription was expected. RT-qPCR analysis confirmed that *Acox1* mRNA level was not modified (data not shown). The disruption of the *Acox1* gene in the mutant cell clone was confirmed by western blot analysis demonstrating the absence of ACOX1 protein (Fig. 2). The typical pattern of ACOX1 expression was observed in WT BV-2 cell lysate (one band at 72 kDa corresponding to the full-length protein (661 aa) and one shorter band at 50 kDa corresponding to a post-translationally cleaved subunit). Despite the presence of several weakly cross-reacting proteins observed both in WT and mutant cell lysate, the specific bands were clearly absent in the BV-2 mutant cell clone confirming the knockout.

To functionally validate the *Acox1*-deficient BV-2 cell clone, we monitored peroxisomal β-oxidation by measuring cyanide-insensitive palmitoyl-CoA oxidation in total cell extracts (Fig. 3A). As expected, the absence of ACOX1 protein resulted in a virtually null enzymatic activity. Since catalase, a H_2O_2-degrading enzyme, is known as the most abundant protein in peroxisomes, we measured its activity in the same extracts. *Acox1*-deficient cells displayed a 2.5-fold higher activity than control cells (Fig. 3B).

3.2. Cell morphology and growth curve of the Acox1-deficient BV-2 cell line

One of the features observed in skin fibroblasts derived from patients with a mutation in the *ACOX1* gene was striking slow-growth compared to control skin fibroblasts [21]. We thus explored whether *Acox1* knockout could trigger cellular modifications both in term of morphology and cell proliferation. Growth of *Acox1*-deficient BV-2 cells was analyzed over a period of 4 days and compared to WT BV-2 cells (Fig. 4). The number of cells was quite similar at 24 h. At 72 h, the number of WT cells was almost double of mutant cells suggesting a slower division time in mutant cells. Cells reached a plateau phase at 96 h in both cases. The mortality was almost identical between BV-2 WT cells and *Acox1*-deficient cells (data not shown).

Regarding the cell morphology, we did not observe obvious differences between WT and mutant BV-2 cells [37]. The majority of mutant cells exhibited a round shape typical of a microglial activated status (Fig. 5A-B). Less than 5% of cells showed an elongated shape with ramifications. To extend our observations, we further analyzed the *Acox1*-deficient BV-2 cells by electron microscopy using diaminobenzidine (DAB) staining, which allows cytochemical detection of peroxisomes (Fig. 5C-H). In comparison with the WT cells, we observed a statistically significant increased number of peroxisomes (1.89-fold) suggesting peroxisome proliferation and/or alteration of pexophagy mechanisms. Peroxisomal staining in mutant cells was more pronounced, which could be linked to the increased catalase activity as shown in Fig. 3B. The peroxisomal average areas were not significantly different (0.0382 μm^2 +/- 0.0030 in WT cells (n=50) vs 0.0368 μm^2 +/- 0.0026 in *Acox1*-deficient cells (n=68)). No obvious change in mitochondrial shape was observed, except for the presence of elongated organelles, suggesting fission. Mitochondria areas were found significantly reduced (0.603 μm^2 +/- 0.034 in WT cells (n=133) vs 0.502 μm^2 +/- 0.020 *Acox1*-deficient cells (n=240)) and their number was significantly increased in mutant cells (1.66-fold). Control and mutant cells showed the presence of lipid droplets. Interestingly, some mutant cells seemed to present an overload of neutral lipids as suggested by the more intense Oil red O staining (Fig. 5I-J).

3.3. Consequences of the absence of ACOX1 activity on fatty acid levels in the Acox1-deficient BV-2 cell line

Actually, accumulation of lipids was expected in *Acox1*-deficient cells since the absence of ACOX1 activity is supposed to yield accumulation of VLCFA. We thus conducted a lipid analysis to compare the levels of fatty acids in WT and *Acox1*-deficient BV-2 cells. As shown in table 2, the total fatty acid levels as well as the global quantity of the main species of fatty acids analyzed (saturated, mono-unsaturated and poly-unsaturated fatty acids) did not present significant differences between mutant and control cells. However, C26:0 and C24:0 levels, which represent a very low percentage of total saturated fatty acids, were found significantly increased in the *Acox1*-deficient cells (x3.5 for C26:0 and x1.6 for C24:0). The C26:0/C22:0 and C24:0/C22:0 ratio, which are used as diagnosis biochemical markers for peroxisomal disorders were respectively 3- and 1.4-fold higher than the control ones (Fig. 6). Monounsaturated fatty acid levels were also significantly modified. A significant increase was observed for C16:1 n-7, C20:1 n-9, C22:1 n-9, C24:1 n-9 and C26:1 n-9 levels while C18:1 n-9 levels were found decreased. Concerning polyunsaturated fatty acids, we noticed a decreased level of C20:5 n-3 and an increased level of C18:2 n-6. Docosahexaenoic acid (DHA, C22:6 n-3) and arachidonic acid (AA, C20:4 n-6) levels remained almost unchanged.

3.4. Expression of key microglial genes in the Acox1-deficient BV-2 cell line

As stated in the introduction, microglial cells ensure an important role in brain homeostasis by controlling inflammation and participating to phagocytosis of apoptotic cells and myelin debris. As a preliminary study of the functional consequences of ACOX1 deficiency in the BV-2 cells, we investigated the mRNA levels of genes encoding interleukin-1β and 6 (IL-1β and IL-6), two major inflammatory cytokines in the brain recognized as polarization markers of microglia [38, 39], and the membrane receptor called triggering receptor expressed by myeloid cells-2 (Trem2), which controls the phenotypic conversion of microglia and promotes phagocytosis [40]. Interestingly, *IL-1β* and *Trem2* expression levels were significantly increased while *IL-6* expression level was significantly decreased (Fig. 7).

Discussion

In this study, we used CRISPR/Cas9 technology to knock out the *Acox1* gene in BV-2 cells, a cell line commonly used as a substitute for primary microglia. Among the 52 cell clones

isolated, we failed in obtaining biallelic HDR. The targeted integration into a single allele must be related to the fact that mammalian cells have a higher frequency of NHEJ events than HDR events and that we target the transcriptionally active strand. Recent studies suggest that the targeting of transcriptionally inactive strand would improve the frequency of homologous recombination [41]. Altogether, we isolated a dozen clones with monoallelic recombination and found the same single mutation in all the clones analyzed, a T nucleotide insertion resulting in a sequence frameshift. It is possible that the 12 clones derived from a single parental cell by mitotic cell division. We selected one clone for further Cre transfection to remove the selection cassette. Sorted cell clones after Cre transfection were screened by PCR and sequencing to confirm efficient Cre recombination. The *Acox1* knockout was confirmed by western blotting in one selected cell clone that was further amplified to obtain a large stock of cryogenic vials at the lowest passage. The chosen strategy facilitated the selection of knockout cells with a fluorescent reporter and antibiotics. In addition, the strategy offered the advantage of expressing Cas9 nuclease for a short duration, thus reducing the risk of off-target events, while remaining effective.

We first confirmed mutations by DNA sequencing as well as the absence of ACOX1 protein by western blotting, but it remained to validate the loss of enzymatic activity and the main biochemical characteristic of ACOX1 deficiency, i.e. VLCFA accumulation. There are indeed numerous examples of knockouts, which present no or subtle phenotype due to compensatory effects and redundant genes. In this case, possible compensation for the absence of ACOX1 by ACOX2 or ACOX3 was unlikely due to non-overlapping substrate specificities [42]. Measurement of palmitoyl-CoA oxidation demonstrated the virtual absence of enzymatic activity in *Acox1*-deficients cell extracts while catalase activity was found increased. This apparent paradox was previously reported in the liver of *Acox1*$^{-/-}$ mice [43] or after specific inhibition of ACOX1 activity in rats [44]. Actually, such an increase could be caused by a change in RedOx status as previously reported in *Acox1*$^{-/-}$ mice by the increase of hepatic H_2O_2 level [45] and since catalase expression and activity are indeed very sensitive to oxidative stress [46]. *Acox1* deficiency in mice or *Acox1* silencing in 158N oligodendrocytes have indeed been proven to generate oxidative stress [47, 48]. Epigenetic or post-transcriptional regulations may be considered as possible explanations of the increased catalase activity [46]. Given the increased number of peroxisomes and mitochondria and the decreased size of mitochondria observed in *Acox1*-defcient cells, a possible activation of PPARα would also make sense. Peroxisomes and mitochondria share very similar division and proliferation mechanisms that depend in part on PPARα activation [49]. In the *Acox1*$^{-/-}$ mice liver, a sustained activation of PPARα pathways has been observed [11, 45]. The most admitted hypothesis is that one or several substrates of ACOX1 accumulate and serve as PPARα activators [50]. Among these substrates, VLCFA have been described as PPARα ligands [51, 52]. The lipid analysis of *Acox1*-deficient cells confirmed the accumulation of VLCFA (C26:0, C24:0, C26:1, C24:1). Other ligands and putative activators such as PUFA and MUFA or phospholipids containing MUFA have been described [53-55]. While we noticed some modifications of the MUFA levels in *Acox1*-deficient cells, no obvious modifications of PUFA were observed in contrast to patient fibroblasts or *Acox1*$^{-/-}$ mice in which plasma levels of DHA and AA were decreased [56, 57]. In our cell model, a preliminary analysis of PPARα responsive genes such as *Acox1* or *Pex11b* showed a weak induction that does not support clearly the involvement of PPARα (data not shown). Of note, PPARα–independent mechanisms of peroxisomal proliferation have previously been described [49, 58, 59]. The transcriptomic analysis, which is in progress, will help to confirm this hypothesis and delineate the causative pathway.

When developing a rodent cell model with the objective to study human diseases, it is always important to ensure that the main markers of the disease are found. Here, we can argue that the variations in saturated and monounsaturated VLCFA levels observed in BV-2 mutant

cells are in the low range but of the same order as those observed in skin fibroblasts and plasma of patients with ACOX1 deficiency [16, 60, 61]. Moreover, the observed modifications of lipid droplet distribution in the mutant cells is consistent with what was observed in the liver of patients with ACOX1 defect and *Acox1*$^{-/-}$ mice [56]. Accumulation of neutral lipids, mainly cholesteryl-esters, seems to represent a hallmark of peroxisomal biogenesis disorders or single peroxisomal gene defects such as ACOX1 deficiency or X-linked adrenoleukodystrophy. Oil red O staining in *Acox1*-deficient BV-2 cells suggests such accumulation. Of note, similar results had been obtained in 158N oligodendrocytes upon *Acox1* silencing [48]. Further in-depth analysis of lipid content in the *Acox1*-deficient cells will permit to precise the nature of the accumulated lipids and establish whether the peroxisomal defect has also consequences on membrane lipids. It is tempting to speculate that membrane modifications of these microglial cells may disrupt their phagocytosis capacity and antigenic presentation function. Moreover, because of the role of microglia in brain homeostasis and inflammation control, further lipid analysis should also focus on signaling molecules of lipid origin secreted by microglial cells, i.e. docosanoid and eicosanoids fatty acid derivatives, which are tightly connected to peroxisomal metabolism [62].

The absence of peroxisome proliferation in human fibroblasts [21] represents a discrepancy with our results but the absence of PPARα response to peroxisome proliferators in human skin fibroblasts may explain this observation [58]. Moreover, enlarged peroxisomes were observed in human liver [63] while we found almost no change in size in the present study. Further analysis is needed to clarify this point which is probably associated with tissue or species differences. Noteworthy, even in a same tissue, i.e. the liver, peroxisomal proliferation as well as the peroxisomal size was found to vary with the age of *Acox1*$^{-/-}$ mice [45].

Very interestingly, in the absence of any stimuli, we found that the expression levels of genes expressing the proinflammatory cytokines (IL-1β and IL-6) and the cell surface protein Trem2 which controls microglial polarization and inflammatory response, are modified in *Acox1*-deficient cells. Induction of *IL-1β* and *IL-6* was described in BV-2 cells upon LPS stimulation [64]. The observed induction of *IL-1β* and the repression of *IL-6* is unusual and suggests that the peroxisomal defect triggered a singular activated state. Further experiments will be needed to extend these observations and confirm this particular activated state as well as a possible modification of the phagocytic ability of these cells. The induction of *Trem2*, whose positive role in phagocytosis is well established [40], indeed suggests that *Acox1*-deficiency may modify the phagocytosis ability.

Conclusion

In summary, by using CRISPR/Cas9 editing, we have generated an *Acox1*-deficient microglial cell line whose preliminary characterization confirms the main biochemical observations made in *Acox1*$^{-/-}$ mice models and skin fibroblasts of patients, i.e. the accumulation of VLCFA. The preliminary study of the mutant cells revealed subcellular modifications in peroxisomes and mitochondria and modifications of the expression of key microglial genes, which let suppose that peroxisomal defect triggers profound changes in microglial functions. Transcriptomic RNAseq analysis is in progress to confirm these observations and reveal putative other dysregulated genes involved in RedOx homeostasis and inflammatory responses. This novel cell model will offer the advantage to test the impact of ACOX1 deficiency in a key cell type for neurodegenerative process and to test original hypotheses on the involvement of peroxisome in phagocytosis, inflammatory and immune response. Microglial mutant cells will offer opportunities to further progress in the understanding of the physiopathogenesis of peroxisomal leukodystrophies.

Acknowledgments
This work was supported by the Ministère de l'Education Nationale et de l'Enseignement Supérieur et de la Recherche (France) and by institutional grants from INSERM, CNRS and Aix-Marseille University to the CIML. Quentin Raas received a fellowship from ARSEP (Association for Research on Multiple Sclerosis). Fatima Saih received a fellowship "Action Intégrée of the Comité Mixte Inter-universitaire Franco-Marocain" (CMIFM, AIMA/14/310, Campus France N° 30293PA) from the PHC Toubkal program, Ministère des Affaires Etrangères. We thank the DImaCell platform for technical assistance in TEM (Microscopy Centre INRA/UB) and the cytometry platform of Dijon for cell sorting (INSERM/UB). We acknowledge the PICSL imaging facility of the CIML (ImagImm), member of the national infrastructure France-BioImaging supported by the French National Research Agency (ANR-10-INBS-04). We thank Myriam Baes for providing us the Cre expression vector as well as Hai Tao He and Didier Marguet for hosting Quentin Raas for a few months at CIML.

References

[1] J. Vamecq, M. Cherkaoui-Malki, P. Andreoletti, N. Latruffe, The human peroxisome in health and disease: the story of an oddity becoming a vital organelle, Biochimie 98 (2014) 4-15.
[2] R.J. Wanders, H.R. Waterham, Biochemistry of mammalian peroxisomes revisited, Annu. Rev. Biochem. 75 (2006) 295-332.
[3] E. Baumgart, J.C. Vanhooren, M. Fransen, P. Marynen, M. Puype, J. Vandekerckhove, J.A. Leunissen, H.D. Fahimi, G.P. Mannaerts, P.P. van Veldhoven, Molecular characterization of the human peroxisomal branched-chain acyl-CoA oxidase: cDNA cloning, chromosomal assignment, tissue distribution, and evidence for the absence of the protein in Zellweger syndrome, Proc. Natl. Acad. Sci. U.S.A. 93 (1996) 13748-13753.
[4] S. Ferdinandusse, S. Denis, C.W.T. van Roermund, M.A. Preece, J. Koster, M.S. Ebberink, H.R. Waterham, R.J.A. Wanders, A novel case of ACOX2 deficiency leads to recognition of a third human peroxisomal acyl-CoA oxidase, Biochim. Biophys. Acta. 1864 (2018) 952-958.
[5] L. Schepers, P.P. Van Veldhoven, M. Casteels, H.J. Eyssen, G.P. Mannaerts, Presence of three acyl-CoA oxidases in rat liver peroxisomes. An inducible fatty acyl-CoA oxidase, a noninducible fatty acyl-CoA oxidase, and a noninducible trihydroxycoprostanoyl-CoA oxidase, J. Biol. Chem. 265 (1990) 5242-5246.
[6] T. Aoyama, I. Ueno, T. Kamijo, T. Hashimoto, Rat very-long-chain acyl-CoA dehydrogenase, a novel mitochondrial acyl-CoA dehydrogenase gene product, is a rate-limiting enzyme in long-chain fatty acid beta-oxidation system. cDNA and deduced amino acid sequence and distinct specificities of the cDNA-expressed protein, J. Biol. Chem. 269 (1994) 19088-19094.
[7] B. Fournier, J.M. Saudubray, B. Benichou, S. Lyonnet, A. Munnich, H. Clevers, B.T. Poll-The, Large deletion of the peroxisomal acyl-CoA oxidase gene in pseudoneonatal adrenoleukodystrophy, J. Clin. Invest. 94 (1994) 526-531.
[8] C. Nohammer, Y. El-Shabrawi, S. Schauer, M. Hiden, J. Berger, S. Forss-Petter, E. Winter, R. Eferl, R. Zechner, G. Hoefler, cDNA cloning and analysis of tissue-specific expression of mouse peroxisomal straight-chain acyl-CoA oxidase, Eur. J. Biochem. 267 (2000) 1254-1260.
[9] U. Varanasi, R. Chu, S. Chu, R. Espinosa, M.M. LeBeau, J.K. Reddy, Isolation of the human peroxisomal acyl-CoA oxidase gene: organization, promoter analysis, and chromosomal localization, Proc. Natl. Acad. Sci. U.S.A. 91 (1994) 3107-3111.

[10] D. Oaxaca-Castillo, P. Andreoletti, A. Vluggens, S. Yu, P.P. van Veldhoven, J.K. Reddy, M. Cherkaoui-Malki, Biochemical characterization of two functional human liver acyl-CoA oxidase isoforms 1a and 1b encoded by a single gene, Biochem. Biophys. Res. Commun. 360 (2007) 314-319.
[11] C.Y. Fan, J. Pan, R. Chu, D. Lee, K.D. Kluckman, N. Usuda, I. Singh, A.V. Yeldandi, M.S. Rao, N. Maeda, J.K. Reddy, Hepatocellular and hepatic peroxisomal alterations in mice with a disrupted peroxisomal fatty acyl-coenzyme A oxidase gene, J. Biol. Chem. 271 (1996) 24698-24710.
[12] S. Farioli-Vecchioli, S. Moreno, M.P. Ceru, Immunocytochemical localization of acyl-CoA oxidase in the rat central nervous system, J. Neurocytol. 30 (2001) 21-33.
[13] F. Fouquet, J.M. Zhou, E. Ralston, K. Murray, F. Troalen, E. Magal, O. Robain, M. Dubois-Dalcq, P. Aubourg, Expression of the adrenoleukodystrophy protein in the human and mouse central nervous system, Neurobiol. Dis. 3 (1997) 271-285.
[14] B.T. Poll-The, F. Roels, H. Ogier, J. Scotto, J. Vamecq, R.B. Schutgens, R.J. Wanders, C.W. van Roermund, M.J. van Wijland, A.W. Schram, e. al, A new peroxisomal disorder with enlarged peroxisomes and a specific deficiency of acyl-CoA oxidase (pseudo-neonatal adrenoleukodystrophy), Am. J. Hum. Genet. 42 (1988) 422-434.
[15] Y. Suzuki, N. Shimozawa, S. Yajima, S. Tomatsu, N. Kondo, Y. Nakada, S. Akaboshi, M. Lai, Y. Tanabe, T. Hashimoto, et al., Novel subtype of peroxisomal acyl-CoA oxidase deficiency and bifunctional enzyme deficiency with detectable enzyme protein: identification by means of complementation analysis, Am. J. Hum. Genet. 54 (1994) 36-43.
[16] S. Ferdinandusse, S. Denis, E.M. Hogenhout, J. Koster, C.W. van Roermund, I.J. L, A.B. Moser, R.J. Wanders, H.R. Waterham, Clinical, biochemical, and mutational spectrum of peroxisomal acyl-coenzyme A oxidase deficiency, Hum. Mutat. 28 (2007) 904-912.
[17] R.Y. Wang, E.S. Monuki, J. Powers, P.H. Schwartz, P.A. Watkins, Y. Shi, A. Moser, D.A. Shrier, H.R. Waterham, D.J. Nugent, J.E. Abdenur, Effects of hematopoietic stem cell transplantation on acyl-CoA oxidase deficiency: a sibling comparison study, J. Inherit. Metab. Dis. 37 (2014) 791-799.
[18] C. Van den Branden, J. Leeman, G. Dacremont, R. Collumbien, F. Roels, Experimental inhibition of peroxisomal beta-oxidation in rats: influence on brain myelination, Glia 3 (1990) 458-463.
[19] P.A. Watkins, M.C. McGuinness, G.V. Raymond, B.A. Hicks, J.M. Sisk, A.B. Moser, H.W. Moser, Distinction between peroxisomal bifunctional enzyme and acyl-CoA oxidase deficiencies, Ann. Neurol. 38 (1995) 472-477.
[20] R.J. Wanders, A. Schelen, N. Feller, R.B. Schutgens, F. Stellaard, C. Jakobs, B. Mitulla, G. Seidlitz, First prenatal diagnosis of acyl-CoA oxidase deficiency, J. Inherit. Metab. Dis. 13 (1990) 371-374.
[21] H.I. El Hajj, A. Vluggens, P. Andreoletti, K. Ragot, S. Mandard, S. Kersten, H.R. Waterham, G. Lizard, R.J. Wanders, J.K. Reddy, M. Cherkaoui-Malki, The inflammatory response in acyl-CoA oxidase 1 deficiency (pseudoneonatal adrenoleukodystrophy), Endocrinol. 153 (2012) 2568-2575.
[22] A. Bottelbergs, S. Verheijden, L. Hulshagen, D.H. Gutmann, S. Goebbels, K.A. Nave, C. Kassmann, M. Baes, Axonal integrity in the absence of functional peroxisomes from projection neurons and astrocytes, Glia 58 (2010) 1532-1543.
[23] L. Hulshagen, O. Krysko, A. Bottelbergs, S. Huyghe, R. Klein, P.P. Van Veldhoven, P.P. De Deyn, R. D'Hooge, D. Hartmann, M. Baes, Absence of functional peroxisomes from mouse CNS causes dysmyelination and axon degeneration, J. Neurosci. 28 (2008) 4015-4027.

[24] C.M. Kassmann, C. Lappe-Siefke, M. Baes, B. Brugger, A. Mildner, H.B. Werner, O. Natt, T. Michaelis, M. Prinz, J. Frahm, K.A. Nave, Axonal loss and neuroinflammation caused by peroxisome-deficient oligodendrocytes, Nat. Genet. 39 (2007) 969-976.
[25] Y. Gong, N. Sasidharan, F. Laheji, M. Frosch, P. Musolino, R. Tanzi, D.Y. Kim, A. Biffi, J. El Khoury, F. Eichler, Microglial dysfunction as a key pathological change in adrenomyeloneuropathy, Ann. Neurol. 82 (2017) 813-827.
[26] F.S. Eichler, J.Q. Ren, M. Cossoy, A.M. Rietsch, S. Nagpal, A.B. Moser, M.P. Frosch, R.M. Ransohoff, Is microglial apoptosis an early pathogenic change in cerebral X-linked adrenoleukodystrophy?, Ann. Neurol. 63 (2008) 729-742.
[27] M. Kocur, R. Schneider, A.K. Pulm, J. Bauer, S. Kropp, M. Gliem, J. Ingwersen, N. Goebels, J. Alferink, T. Prozorovski, O. Aktas, S. Scheu, IFNbeta secreted by microglia mediates clearance of myelin debris in CNS autoimmunity, Acta. Neuropathol. Commun. 3 (2015) 20.
[28] M. Jinek, K. Chylinski, I. Fonfara, M. Hauer, J.A. Doudna, E. Charpentier, A programmable dual-RNA-guided DNA endonuclease in adaptive bacterial immunity, Science 337 (2012) 816-821.
[29] E. Blasi, R. Barluzzi, V. Bocchini, R. Mazzolla, F. Bistoni, Immortalization of murine microglial cells by a v-raf/v-myc carrying retrovirus, J. Neuroimmunol. 27 (1990) 229-237.
[30] A. Henn, S. Lund, M. Hedtjarn, A. Schrattenholz, P. Porzgen, M. Leist, The suitability of BV2 cells as alternative model system for primary microglia cultures or for animal experiments examining brain inflammation, Altex 26 (2009) 83-94.
[31] V. Bocchini, R. Mazzolla, R. Barluzzi, E. Blasi, P. Sick, H. Kettenmann, An immortalized cell line expresses properties of activated microglial cells, J. Neurosci. Res. 31 (1992) 616-621.
[32] V. Pattanayak, S. Lin, J.P. Guilinger, E. Ma, J.A. Doudna, D.R. Liu, High-throughput profiling of off-target DNA cleavage reveals RNA-programmed Cas9 nuclease specificity, Nat. Biotechnol. 31 (2013) 839-843.
[33] Z. El Kebbaj, P. Andreoletti, D. Mountassif, M. Kabine, H. Schohn, M. Dauca, N. Latruffe, M.S. El Kebbaj, M. Cherkaoui-Malki, Differential regulation of peroxisome proliferator-activated receptor (PPAR)-alpha1 and truncated PPARalpha2 as an adaptive response to fasting in the control of hepatic peroxisomal fatty acid beta-oxidation in the hibernating mammal, Endocrinol. 150 (2009) 1192-1201.
[34] P.B. Lazarow, C. De Duve, A fatty acyl-CoA oxidizing system in rat liver peroxisomes; enhancement by clofibrate, a hypolipidemic drug, Proc. Natl. Acad. Sci. U.S.A. 73 (1976) 2043-2046.
[35] J. Ni, S. Tokuyama, A. Sogabe, Y. Kawamura, Y. Tahara, Cloning and high expression of catalase gene from bacillus sp. TE124, J. Biosci. Bioeng. 91 (2001) 422-424.
[36] C. Gondcaille, E.C. Genin, T.E. Lopez, A.M. Dias, F. Geillon, P. Andreoletti, M. Cherkaoui-Malki, T. Nury, G. Lizard, I. Weinhofer, J. Berger, E.T. Kase, D. Trompier, S. Savary, LXR antagonists induce ABCD2 expression, Biochim. Biophys. Acta. 1841 (2014) 259-266.
[37] M.A. Laurenzi, C. Arcuri, R. Rossi, P. Marconi, V. Bocchini, Effects of microenvironment on morphology and function of the microglial cell line BV-2, Neurochem. Res. 26 (2001) 1209-1216.
[38] X. Liu, N. Quan, Microglia and CNS Interleukin-1: Beyond Immunological Concepts, Frontiers in neurology 9 (2018) 8.
[39] M. Erta, A. Quintana, J. Hidalgo, Interleukin-6, a major cytokine in the central nervous system, Int J Biol Sci 8 (2012) 1254-1266.
[40] T.R. Jay, V.E. von Saucken, G.E. Landreth, TREM2 in Neurodegenerative Diseases, Mol. Neurodegener. 12 (2017) 56.

[41] F. Song, K. Stieger, Optimizing the DNA donor template for homology-directed repair of double-strand breaks, Mol. Ther. Nucleic Acids 7 (2017) 53-60.
[42] P.P. Van Veldhoven, Biochemistry and genetics of inherited disorders of peroxisomal fatty acid metabolism, J. Lipid Res. 51 (2010) 2863-2895.
[43] R. Chu, H. Lim, L. Brumfield, H. Liu, C. Herring, P. Ulintz, J.K. Reddy, M. Davison, Protein profiling of mouse livers with peroxisome proliferator-activated receptor alpha activation, Mol. Cell. Biol. 24 (2004) 6288-6297.
[44] J. Zeng, S. Deng, Y. Wang, P. Li, L. Tang, Y. Pang, Specific inhibition of acyl-CoA oxidase-1 by an acetylenic acid improves hepatic lipid and reactive oxygen species (ROS) metabolism in rats fed a high fat diet, J. Biol. Chem. 292 (2017) 3800-3809.
[45] C.Y. Fan, J. Pan, N. Usuda, A.V. Yeldandi, M.S. Rao, J.K. Reddy, Steatohepatitis, spontaneous peroxisome proliferation and liver tumors in mice lacking peroxisomal fatty acyl-CoA oxidase. Implications for peroxisome proliferator-activated receptor alpha natural ligand metabolism, J. Biol. Chem. 273 (1998) 15639-15645.
[46] C. Glorieux, M. Zamocky, J.M. Sandoval, J. Verrax, P.B. Calderon, Regulation of catalase expression in healthy and cancerous cells, Free Radical Biol. Med. 87 (2015) 84-97.
[47] J. Huang, N. Viswakarma, S. Yu, Y. Jia, L. Bai, A. Vluggens, M. Cherkaoui-Malki, M. Khan, I. Singh, G. Yang, M.S. Rao, J. Borensztajn, J.K. Reddy, Progressive endoplasmic reticulum stress contributes to hepatocarcinogenesis in fatty acyl-CoA oxidase 1-deficient mice, Am. J. Pathol. 179 (2011) 703-713.
[48] M. Baarine, P. Andreoletti, A. Athias, T. Nury, A. Zarrouk, K. Ragot, A. Vejux, J.M. Riedinger, Z. Kattan, G. Bessede, D. Trompier, S. Savary, M. Cherkaoui-Malki, G. Lizard, Evidence of oxidative stress in very long chain fatty acid-treated oligodendrocytes and potentialization of ROS production using RNA interference-directed knockdown of ABCD1 and ACOX1 peroxisomal proteins, Neurosci. 213 (2012) 1-18.
[49] M. Schrader, J.L. Costello, L.F. Godinho, A.S. Azadi, M. Islinger, Proliferation and fission of peroxisomes - An update, Biochim. Biophys. Acta. 1863 (2016) 971-983.
[50] J. Huang, Y. Jia, T. Fu, N. Viswakarma, L. Bai, M.S. Rao, Y. Zhu, J. Borensztajn, J.K. Reddy, Sustained activation of PPARalpha by endogenous ligands increases hepatic fatty acid oxidation and prevents obesity in ob/ob mice, FASEB J. 26 (2012) 628-638.
[51] H.A. Hostetler, A.B. Kier, F. Schroeder, Very-long-chain and branched-chain fatty acyl-CoAs are high affinity ligands for the peroxisome proliferator-activated receptor alpha (PPARalpha), Biochemistry 45 (2006) 7669-7681.
[52] H.A. Hostetler, A.D. Petrescu, A.B. Kier, F. Schroeder, Peroxisome proliferator-activated receptor alpha interacts with high affinity and is conformationally responsive to endogenous ligands, J. Biol. Chem. 280 (2005) 18667-18682.
[53] B. Grygiel-Gorniak, Peroxisome proliferator-activated receptors and their ligands: nutritional and clinical implications - a review, Nutr. J. 13 (2014) 17.
[54] H. Yokoi, H. Mizukami, A. Nagatsu, H. Tanabe, M. Inoue, Hydroxy monounsaturated fatty acids as agonists for peroxisome proliferator-activated receptors, Biol. Pharm. Bull. 33 (2010) 854-861.
[55] M.V. Chakravarthy, I.J. Lodhi, L. Yin, R.R. Malapaka, H.E. Xu, J. Turk, C.F. Semenkovich, Identification of a physiologically relevant endogenous ligand for PPARalpha in liver, Cell 138 (2009) 476-488.
[56] A. Vluggens, P. Andreoletti, N. Viswakarma, Y. Jia, K. Matsumoto, W. Kulik, M. Khan, J. Huang, D. Guo, S. Yu, J. Sarkar, I. Singh, M.S. Rao, R.J. Wanders, J.K. Reddy, M. Cherkaoui-Malki, Reversal of mouse Acyl-CoA oxidase 1 (ACOX1) null phenotype by human ACOX1b isoform, Lab. Invest. 90 (2010) 696-708.
[57] Y. Abe, M. Honsho, H. Nakanishi, R. Taguchi, Y. Fujiki, Very-long-chain polyunsaturated fatty acids accumulate in phosphatidylcholine of fibroblasts from patients with Zellweger

syndrome and acyl-CoA oxidase1 deficiency, Biochim. Biophys. Acta. 1841 (2014) 610-619.
[58] C. Gondcaille, M. Depreter, S. Fourcade, M. Lecca, S. Leclercq, P. Martin, T. Pineau, F. Cadepond, M. ElEtr, N. Bertrand, A. Beley, S. Duclos, D. De Craemer, F. Roels, S. Savary, M. Bugaut, Phenylbutyrate up-regulates the adrenoleukodystrophy-related gene as a nonclassical peroxisome proliferator, J. Cell Biol. 169 (2005) 93-104.
[59] A. Bagattin, L. Hugendubler, E. Mueller, Transcriptional coactivator PGC-1alpha promotes peroxisomal remodeling and biogenesis, Proc. Natl. Acad. Sci. U.S.A. 107 (2010) 20376-20381.
[60] R. Carrozzo, C. Bellini, S. Lucioli, F. Deodato, D. Cassandrini, M. Cassanello, U. Caruso, C. Rizzo, T. Rizza, M.L. Napolitano, R.J. Wanders, C. Jakobs, C. Bruno, F.M. Santorelli, C. Dionisi-Vici, E. Bonioli, Peroxisomal acyl-CoA-oxidase deficiency: two new cases, Am. J. Med. Genet. A 146A (2008) 1676-1681.
[61] S. Ferdinandusse, S. Barker, K. Lachlan, M. Duran, H.R. Waterham, R.J. Wanders, S. Hammans, Adult peroxisomal acyl-coenzyme A oxidase deficiency with cerebellar and brainstem atrophy, J. Neurol. Neurosurg. Psychiatry 81 (2010) 310-312.
[62] M. Matsuo, Y. Hamasaki, F. Fujiyama, S. Miyazaki, Eicosanoids are produced by microglia, not by astrocytes, in rat glial cell cultures, Brain Res. 685 (1995) 201-204.
[63] I. Kerckaert, D. De Craemer, G. Van Limbergen, Practical guide for morphometry of human peroxisomes on electron micrographs, J. Inherited Metab. Dis. 18 Suppl 1 (1995) 172-180.
[64] Y. Qin, X. Sun, X. Shao, M.X. Hu, J. Feng, Z. Chen, J. Sun, Z. Zhou, Y. Duan, C. Cheng, Lipopolysaccharide Preconditioning Induces an Anti-inflammatory Phenotype in BV2 Microglia, Cell Mol. Neurobiol. 36 (2016) 1269-1277.

Figure Legends

Fig. 1. CRISPR/Cas9-mediated gene knockout strategy and molecular screening in BV-2 cells. (A) Schematic representation of the *Acox1* target locus and donor plasmid allowing homology-directed repair (HDR) and representation of the locus after Cre recombination. The size of amplicons for each case is indicated. The position of primers used for PCR screening are shown by two opposite arrows (HA: homology arm; light grey box: exon 1; dark grey box: plasmid sequence; white boxes: selection cassettes (GFP: green fluorescent protein, Puro: puromycin resistance and TK: thymidine kinase expression); scissors: position of the double strand DNA break). (B) Agarose gel electrophoresis of PCR products (1: negative control; 2: WT; 3: *Acox1* mutant with monoallelic HDR-based mutation; 4: *Acox1* mutant after Cre recombination. Bands corresponding to HDR and either wild type (WT) or non-homologous end joining (NHEJ) repair are indicated. (C) Sanger sequencing results of WT and mutated *Acox1* locus (allele 1 corresponds to NHEJ and allele 2 corresponds to HDR followed by Cre recombination) and gene knockout (boxes: homology arms with annotated positions from the transcription initiation start (+1); grey highlighted sequence: *Acox1* exon 1; bold sequence: sgRNA targeted sequence; underlined sequence: inserted nucleotide; italic: plasmid sequence; *: frameshift mutation; arrows: sequencing primers).

Fig. 2. Western blot analysis of ACOX1 expression in WT and *Acox1*-deficient (-/-) BV-2 cells. Proteins of whole cell lysates were separated on 7.5% SDS-PAGE, blotted on PVDF membrane and analyzed by immunoblotting with anti-ACOX1 and anti-Actin antibodies. The central lane corresponds to molecular weight markers (MWM).

Fig. 3. Cyanide-insensitive palmitoyl-CoA oxidation (A) and catalase activity (B) in WT and *Acox1*-deficient (-/-) BV-2 cells. Data represent the mean +/- SD of 4 independent experiments. Statistically significant differences determined by unpaired t-test analysis are indicated: ** P value ≤ 0.01.

Fig. 4. Proliferation curve of WT and *Acox1*-deficient (-/-) BV-2 cells. At t0, $2x10^4$ cells were seeded. Data represents mean values of 2 independent experiments (cells, from the same passage number, thawed at different dates and cultivated during 48 h) with 3 technical replicates +/- SD. Statistically significant differences determined by ANOVA are indicated: *** P value ≤ 0.001.

Fig. 5. Cell morphology analysis. Phase contrast micrographs of WT (A) and *Acox1*-deficient (B) BV-2 cells showing a majority of round shaped cells and a minority of elongated ramified cells without obvious differences between both genotypes (bar = 20 µm). Transmission electron micrographs (whole cell and respective higher magnification) of WT (C, F) and *Acox1*-deficient (D, G and E, H) BV-2 cells (bar = 2 µm). Peroxisomes and lipid droplets are indicated (arrowheads and short arrows respectively). Mitochondria with elongated shape evoking fission process are indicated by stars. Light microscopic images of Oil Red O staining in WT (I) and *Acox1*-deficient (J) BV-2 cells (bar = 20 µm).

Fig. 6. Relative VLCFA levels in WT and *Acox1*-deficient (-/-) BV-2 cells. The concentrations of the VLCFA species C26∶0, C24∶0 and C22∶0 were determined by GC/MS from WT and mutant BV-2 cells cultivated during 48h. Data represent the mean ratios (C26∶0/C22∶0 and C24∶0/C22∶0) of 3 independent experiments with their respective standard deviation. Fold increase in *Acox1*-deficient BV-2 cells compared to WT is indicated. Statistically significant

differences determined by unpaired t-test analysis are indicated: ** P value ≤ 0.01, * P value ≤ 0.05.

Fig. 7. Relative mRNA levels of key microglial genes in *Acox1*-deficient (-/-) BV-2 cells. Expression levels of genes encoding the inflammatory cytokines (IL-6 and IL-1β) and the phagocytic and immune receptor Trem2 were measured using real time RT-qPCR and normalized to *36B4*. Data represent the mean values +/- SD of 3 experiments and are expressed as relative expression levels in comparison with the corresponding expression level in WT cells taken arbitrary equal to 1. Statistically significant differences determined by unpaired t-test analysis are indicated: ** P value ≤ 0.01, * P value ≤ 0.05.

Table 1. Screening of off-target events in BV-2 *Acox1* mutant cells.

	Sequence	Mismatches (# and position)	Locus
Target sequence	GGCCCGCTCCTTGCGCAGAT**CGG**	4 : [1-2-3-6]	chrX: -7341383
Predicted off-target 1	CTTCCTCTCCTTGCGCAGAT**GGG**		
Target sequence	GGCCCGCTCCTTGCGCAGAT**CGG**	4 : [2-5-7-9]	chr12: -56701554
Predicted off-target 2	GCCAGGT-GCTTGCGCAGAT**AGG**		

Mismatches are underlined and the protospacer adjacent motif (NGG) is in bold.

Table 2. Fatty acid levels in WT and *Acox1*-deficient BV-2 cells cultivated during 48h.

	WT		**ACOX1-/-**			
	Mean	**SD**	**Mean**	**SD**	*p value*	*t-test*
C16:0	**17,716**	2,255	**19,242**	1,087	*0.350*	*NS*
C18:0	**9,925**	1,426	**9,166**	797	*0.466*	*NS*
C20:0	**91.1**	17.6	**104**	14.5	*0.399*	*NS*
C22:0	**28.9**	5.68	**32.7**	5.61	*0.455*	*NS*
C24:0	**62.0**	6.26	**98.4**	14.7	*0.017*	*
C26:0	**11.6**	3.68	**40.6**	3.44	*0.001*	***
SFA	**27,834**	36,834	**28,684**	1,598	*0.733*	*NS*
C16:1 n-7 trans	**1,637**	412	**400**	80.3	*0.007*	**
C16:1 n-7 cis	**5,468**	549	**8,627**	698	*0.004*	**
C18:1 n-9	**24,135**	2,902	**17,776**	1,677	*0.03*	*
C18:1 n-7	**11,012**	860	**12,449**	1,233	*0.173*	*NS*
C20:1 n-9	**330**	22.4	**874**	41.5	*0*	***
C22:1 n-9	**41.5**	4.97	**60.7**	5.89	*0.013*	*
C24:1 n-9	**58.0**	7.50	**91.2**	14.9	*0.026*	*
C26:1 n-9	**15.4**	2.40	**30.7**	4.25	*0.006*	**
MUFA	**42,695**	4,162	**40,308**	3,622	*0.495*	*NS*
C18:2 n-6	**778**	147	**1,255**	251	*0.047*	*
C20:3 n-6	**742**	92.8	**704**	27.8	*0.529*	*NS*
C20:4 n-6	**2,258**	275	**2,586**	199	*0.169*	*NS*
C20:5 n-3	**1,478**	160	**465**	61.2	*0.001*	***
C22:6 n-3	**1,579**	129	**1,295**	150	*0.068*	*NS*
PUFA	**6,836**	778	**6,304**	630	*0.41*	*NS*
Total FA	**77,365**	8,552	**75,296**	5,753	*0.75*	*NS*

Data represent mean levels of fatty acids (saturated (SFA), monounsaturated (MUFA), and polyunsaturated (PUFA)) measured by GC/MS and expressed in ng/mg of protein of 3 independent experiments with their respective standard deviation (SD).
Significant differences at $p \leq 0.001$***, $p \leq 0.01$**, $p \leq 0.05$* determined by unpaired t-test analysis are indicated. NS, not significant.

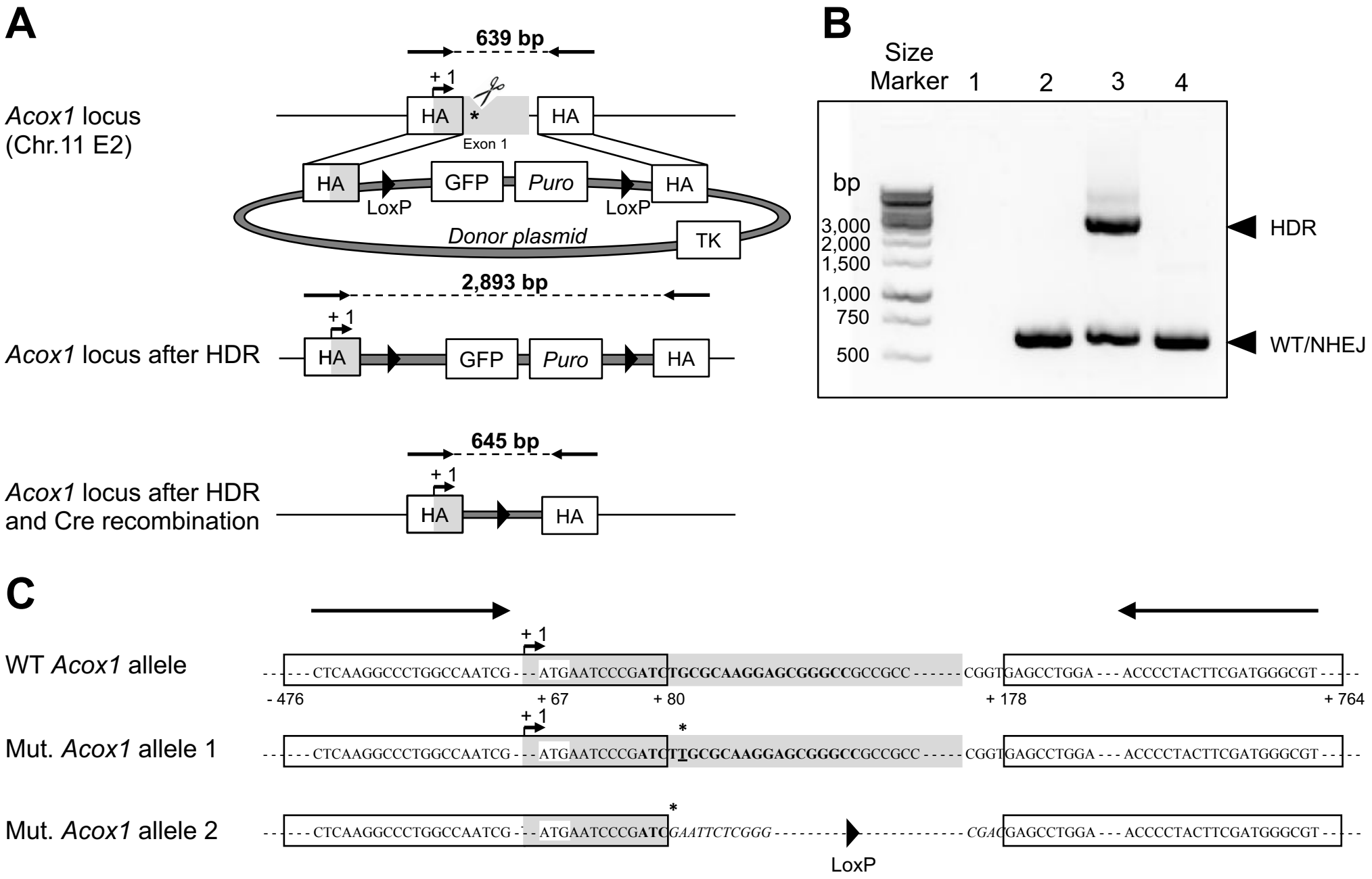
A
639 bp
+ 1
Acox1 locus
(Chr.11 E2)
HA
*
HA
Exon 1
HA
GFP
Puro
HA
LoxP
LoxP
Donor plasmid
TK
2,893 bp
+ 1
Acox1 locus after HDR
HA
GFP
Puro
HA
645 bp
+ 1
Acox1 locus after HDR
and Cre recombination
HA
HA
B
Size
Marker
1
2
3
4
bp
3,000
2,000
1,500
1,000
750
500
HDR
WT/NHEJ
C
WT Acox1 allele
+ 1
CTCAAGGCCCTGGCCAATCG
ATGAATCCCGATCTGCGCAAGGAGCGGGCCGCCGCC
CGGTGAGCCTGGA
ACCCCTACTTCGATGGGCGT
- 476
+ 67
+ 80
+ 178
+ 764
Mut. Acox1 allele 1
+ 1
*
CTCAAGGCCCTGGCCAATCG
ATGAATCCCGATCTTGCGCAAGGAGCGGGCCGCCGCC
CGGTGAGCCTGGA
ACCCCTACTTCGATGGGCGT
Mut. Acox1 allele 2
*
CTCAAGGCCCTGGCCAATCG
ATGAATCCCGATC
GAATTCTCGGG
CGAC
GAGCCTGGA
ACCCCTACTTCGATGGGCGT
LoxP

Fig.1

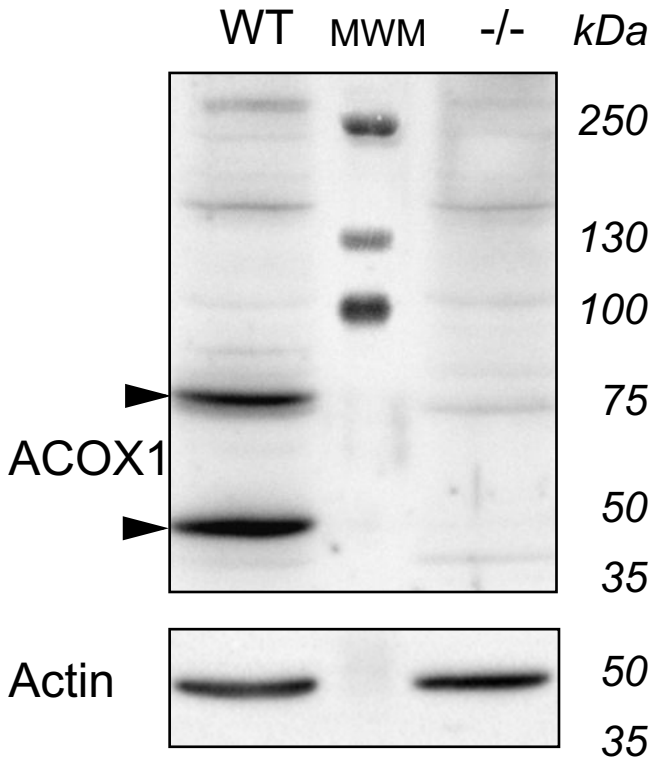

Fig.2

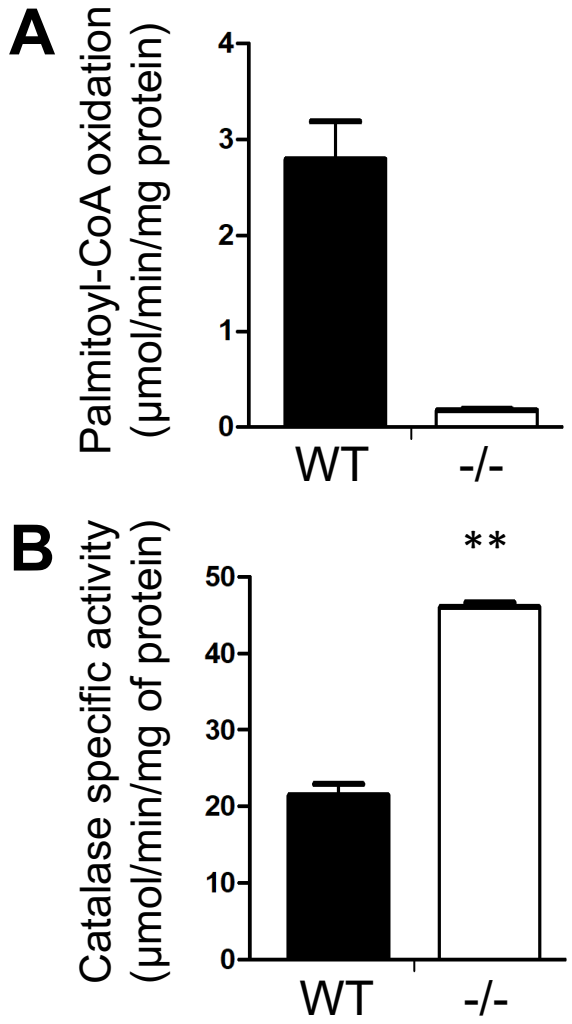
A
Palmitoyl-CoA oxidation
(μmol/min/mg protein)
4
3
2
1
0
WT
-/-
B
Catalase specific activity
(μmol/min/mg of protein)
**
50
40
30
20
10
0
WT
-/-

Fig.3

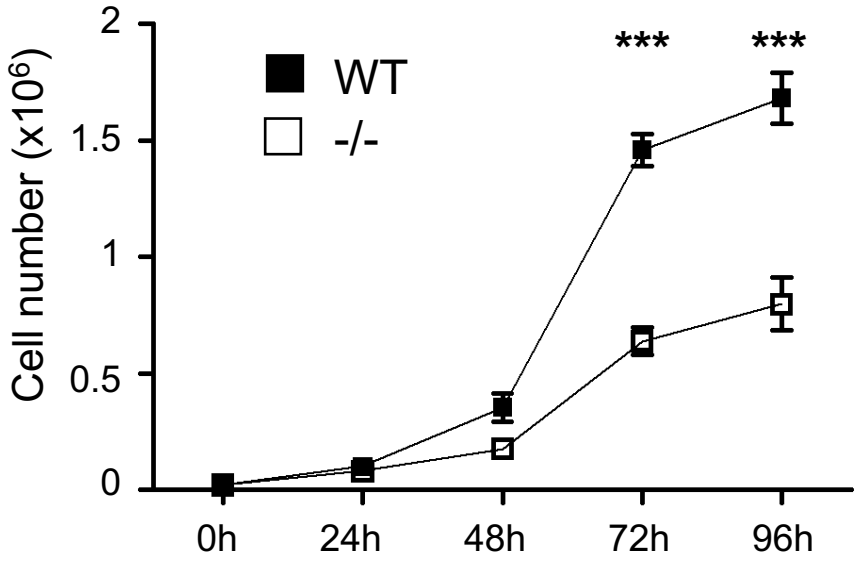

Fig.4

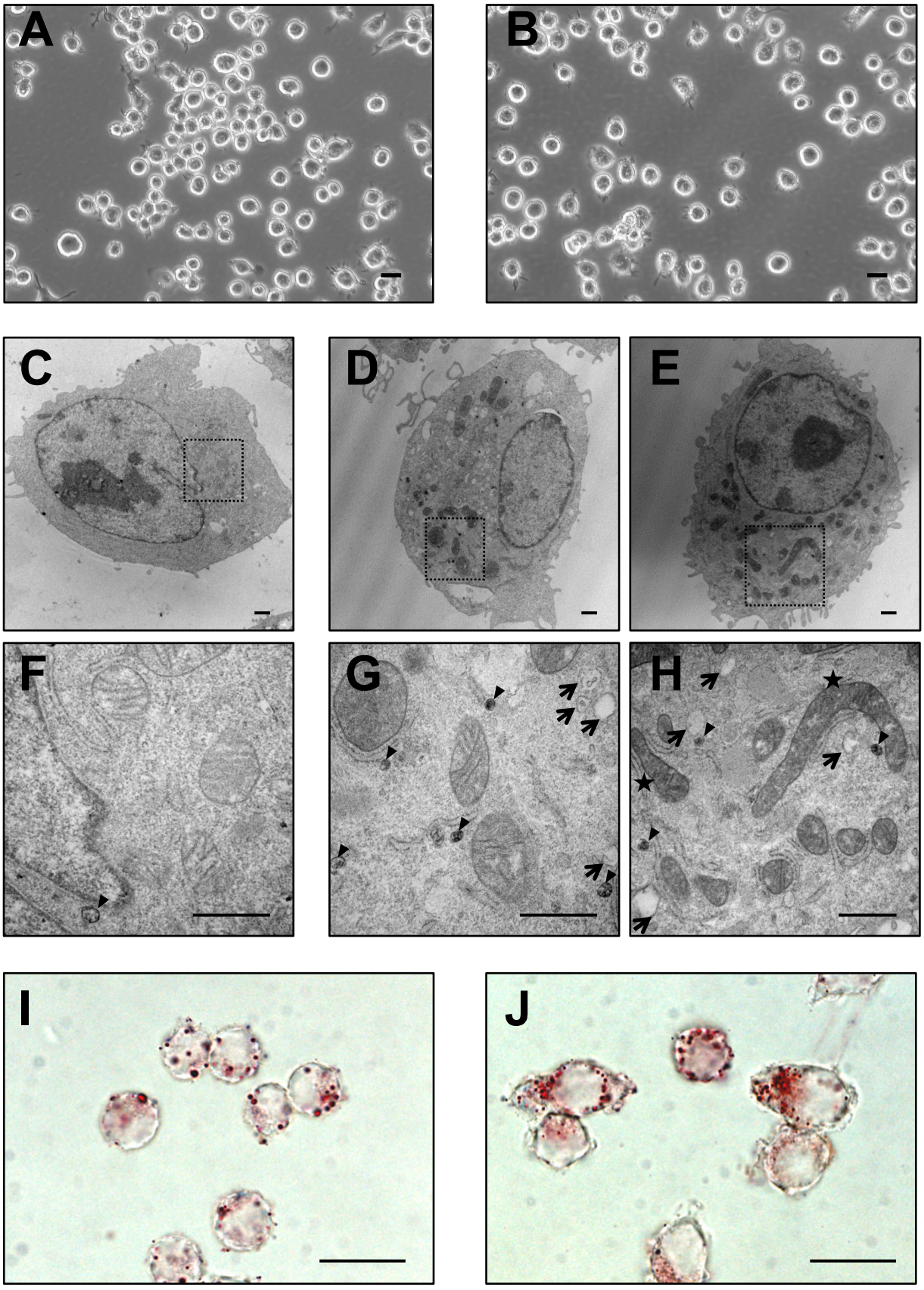

Fig.5

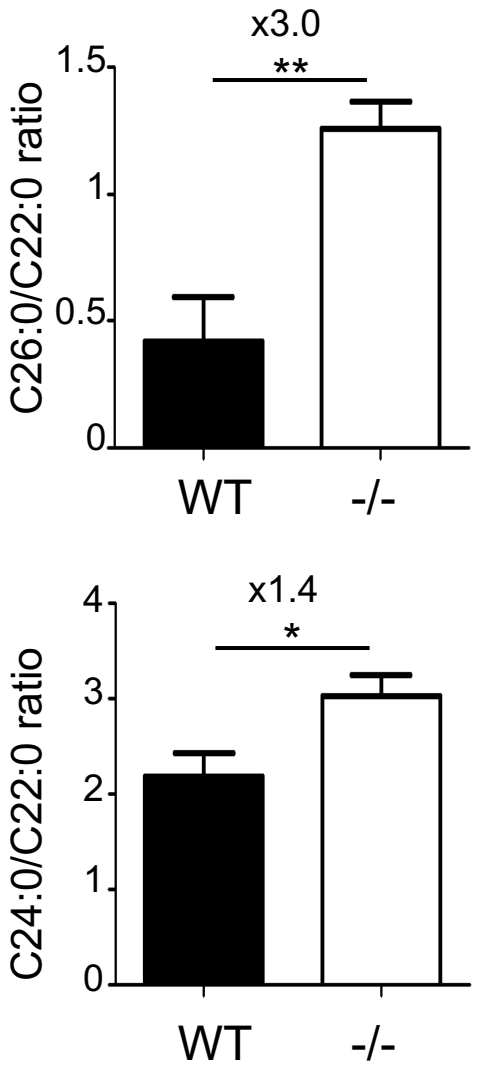

Fig.6

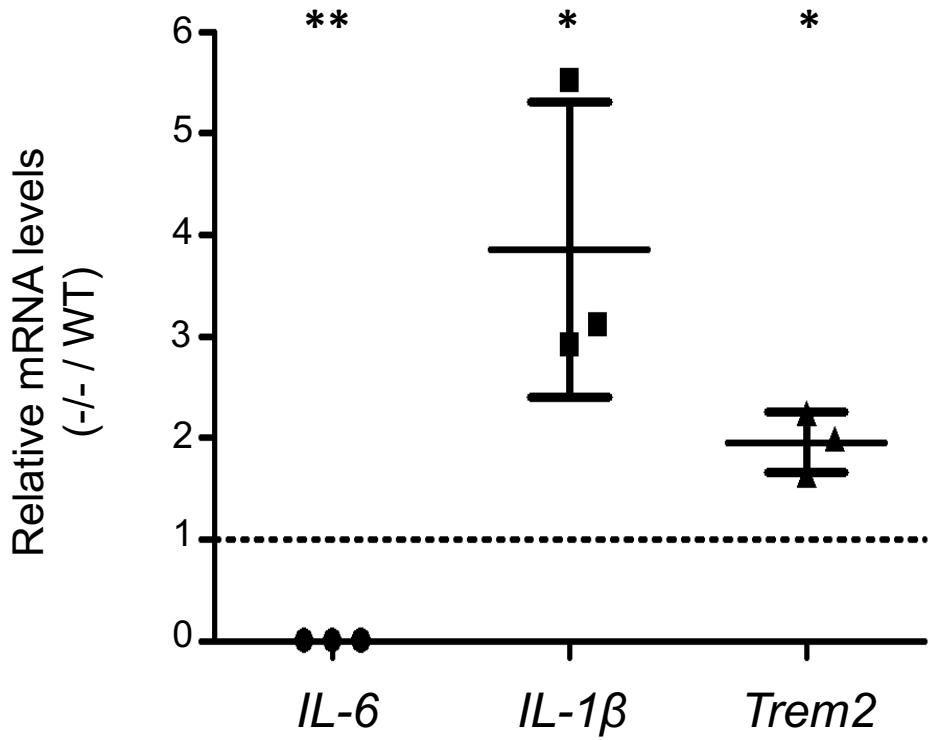

Fig.7